A target group tracking algorithm for wireless sensor networks using azimuthal angle of arrival information*

Zhang Chun(张 淳)[a)b)†], Fei Shu-Min(费树岷)[a)b)], and Zhou Xing-Peng(周杏鹏)[a)b)]

[a)] *School of Automation, Southeast University, Nanjing* 210096, *China*

[b)] *Key Laboratory of Measurement and Control of Complex Systems of Engineering, Ministry of Education, Southeast University, Nanjing* 210096, *China*

(Received 26 April 2012; revised manuscript received 14 June 2012)

In this paper, we explore the technology of tracking a group of targets with correlated motions in a wireless sensor network. Since a group of targets moves collectively and is restricted within a limited region, it is not worth consuming scarce resources of sensors in computing the trajectory of each single target. Hence, in this paper, the problem is modeled as tracking a geographical continuous region covered by all targets. A tracking algorithm is proposed to estimate the region covered by the target group in each sampling period. Based on the locations of sensors and the azimuthal angle of arrival (AOA) information, the estimated region covering all the group members is obtained. Algorithm analysis provides the fundamental limits to the accuracy of localizing a target group. Simulation results show that the proposed algorithm is superior to the existing hull algorithm due to the reduction in estimation error, which is between 10% and 40% of the hull algorithm, with a similar density of sensors. And when the density of sensors increases, the localization accuracy of the proposed algorithm improves dramatically.

Keywords: wireless sensor network, target group, tracking, azimuthal angle, estimation error

PACS: 01.20.+x **DOI:** 10.1088/1674-1056/21/12/120101

1. Introduction

A wireless sensor network (WSN) consists of many intelligent sensor nodes deployed in a monitored region.[1,2] Each sensor is capable of sensing, processing, storing environmental information, and further communicating with other sensors to implement complicated tasks.[3−5] Tracking multiple targets is an important and fundamental subject of wireless sensor networks. Several specific tracking algorithms are proposed in Refs. [6]–[8]. The goal of multi-target tracking is to accurately monitor and obtain the location information of targets moving within the monitored field randomly.

Conventional multi-target tracking problems usually focus on obtaining the trajectory of each individual target. However, in many application areas, a group of targets forming a compact body, called a target group, moves together from one location to another for a common goal. For example, a phalanx of soldiers moves together in a cooperative manner towards their enemy. Under these circumstances, what the end users care about is the trajectory of the mobile community; so it is not necessary to compute the trajectory of each single target. In addition, the targets in the community are close to each other; so it is difficult and inefficient to separately detect and locate each individual target.

A multi-target tracking (MTT) algorithm was proposed in Ref. [6] based on rough and precision association. This algorithm solved the problem of data association. The key idea was to obtain the trajectory of each target by data correlation and state estimation. As mentioned above, it is not worth spending limited resources of sensors on tracking individual targets. Recent studies on WSNs focus on how to track complex targets, such as a two-dimensional (2D) object or a target group. The problem of tracking a 2D object or a target group can be modeled as tracking a geographical continuous region. The original deformable curve model was also used to identify target boundaries.[9,10] Combining the tracking of deformable curves with the identifying of 2D object motivates the tracking of 2D targets with spatiotemporal

*Project supported by the State Key Program of the National Natural Science Foundation of China (Grant No. 60835001), the National Natural Science Foundation of China (Grant No. 61104068), and the Natural Science Foundation of Jiangsu Province, China (Grant No. BK2010200).

†Corresponding author. E-mail: zhc1088@yahoo.cn

© 2012 Chinese Physical Society and IOP Publishing Ltd

properties.[11]

Binary proximity sensors have also been used in the target tracking problem. The advantage of these techniques is that the communication requirements for binary proximity sensors are minimal. However, they are insufficient to accurately estimate the region containing all targets, since the target information obtained from binary sensors is limited. Shrivastava *et al.*[12] explored fundamental performance limits of tracking a target using binary proximity sensors. They used an Occam's razor approach to approximate the trajectory of the target. In Ref. [13], Cao *et al.* employed binary proximity sensors to track a target group. The hull algorithm and the circle (CIR) algorithm were proposed. The main idea of the two algorithms was to provide a monitoring region covering all the targets. However, the monitoring region obtained by the two algorithms may not cover all the group members in the target group.

In this paper, we investigate the problem of tracking the trajectory of a target group. As mentioned in Ref. [14], the problem of tracking a single target was defined as tracking a point where the target is located, whereas the tracking of a target group can be regarded as tracking a geographical continuous region covered by all targets. Hence, one challenging problem is how to estimate the location of the region at different time stamps as the target group moves.

Our contribution in this paper is to provide a tracking algorithm to obtain the geographical regions covering the target group at different time stamps, and minimize the location error. Considering that the AOA is one of the common ranging techniques,[15] here we introduce an AOA-aided target tracking algorithm (ATTC). In the scenario with a single target in the monitored field, applying the AOA technique is to obtain the direction of the received target signal with respect to the orientation. However, in the scenario of tracking a target group, it is not worth consuming scarce resources of sensors to compute the signal direction from each single target. The information we are concerned with is the single angle range. The AOA information dominates the accuracy of trajectory estimation. Based on the AOA information and the locations of sensors, the region covering the target group is estimated in each sampling time. Theoretical analysis provides the fundamental performance limits of the ATTC.

The rest of this paper is organized as follows. In Section 2 we provide the ATTC and explore the fundamental limits to its localization accuracy. Simulation results and concluding remarks are given in Section 3 and Section 4, respectively.

2. Target group tracking algorithm

2.1. Group mobility model

In this section, we describe the mobility model of the target group, called the group mobility model. The group mobility model represents the behaviour of a target group realistically. It attempts to mimic the movement of a real target group.[16]

In this paper, the group mobility model represents a group of targets that move collectively from one location to another. An entity mobility model to move around a logical centre is applied to each target within the target group. The parameters of the entity mobility model determine how far a target can be apart from the logical centre. In this paper, we define the largest distance from a target to the logical center as d_{c}. Hence the radius of the target group is denoted by d_{c}. Here the logical centre is not a real point in a real life system. It is a logical point with which the movements of the targets are correlated. When the logical centre moves from a point to another, all the targets update their locations according to the new location of the logical centre. For example, consider a military scenario, in which a group of soldiers walk together in a cooperative manner to achieve a common goal. Although the shape of region covered by all soldiers is changing, these soldiers surround the logical centre within a given range.

2.2. ATTC

As mentioned in Section 1, the problem of tracking a target group can be modeled as tracking a geographical continuous region covered by all targets. This region is called the actual region. Our object is to design a mechanism to obtain a region covering all targets in sampling times, called the estimated region, and minimize the error between the estimated region and the actual region.

We assume that the ATTC has the following requirements for its operation.

i) The locations of sensors can be recorded when they are deployed, or estimated according to location algorithms.[17]

ii) Sensors sample the target group movement periodically.

iii) We assume that the sensing coverage of sensors in the WSN can cover the monitored area. To make sure that the sensor placement has an ideal coverage, each sensor is assumed to own 4 to 6 close neighbours and then this sensor is called a healthy sensor.[18]

The geometry of target tracking based on AOA is best illustrated via an example. We define a target angle relative to a sensor as the direction of the received target signal with respect to the orientation. As mentioned in Section 1, it is not worth obtaining the angle of each target. What a sensor needs to obtain is the angle range of the targets located within its sensing range. In other words, what a sensor needs to compute is the maximal target angle relative to it and the minimal one. In recent years, the problem related to AOA has been studied.[15,19] Our emphasis is placed on estimating the region covering the target group based on the AOA information. Hence, the problem of how to obtain the angle range is beyond the scope of this paper.

As illustrated in Fig. 1(a), the sensing range of the sensor S_1 is shown as the circle. The angle of target T_1 relative to the sensor S_1 can be expressed as $(\alpha + k * (2\pi))$, where $-2\pi < \alpha < 2\pi$. Hence, each target angle has several expressions as the values of k are different. In this paper, we define the value of k as 0. Then, relative to the sensor S_1, the angle range of the targets within its sensing range is expressed as $[\alpha, \beta]$. Figure 1(b) shows a simple network containing 5 sensors. The circles C_i $(1 \leq i \leq 5)$ represent the sensing ranges of S_i $(1 \leq i \leq 5)$. The actual region covered by the target group is shown as the polygon with dashed line segments. Overlaps between sensing ranges of sensors form many patches. We can see from Fig. 1(b) that the set of patches P_i $(1 \leq i \leq 3)$, which are shown as shaded sections, construct a geographical continuous region, and this region covers the actual region. The estimated region we need to compute is the geographical continuous region formed by the set of patches containing targets. These patches can be obtained based on the AOA information.

The main steps of the ATTC are presented as follows.

Step 1 Obtain the input data

The input data set of the ATTC is an angle range array (ARR). Each element in the ARR contains the location of a sensor which has detected targets, and the angle range within its sensing range. These data packets are sent to a sink node through the multi-hop routing. When the sink node obtains the input data set, it computes the estimated region according to the following steps.

Step 2 Find the sensor which has detected targets with a largest angle range

The large angle range implies that within a sensor sensing range, the difference between the maximal target angle and the minimal one is big. The object of the ATTC is to obtain the set of patches which cover the targets. In order to enhance the efficiency of computation, the sink node first finds the patches contained in the sensing ranges with many targets, and then finds patches in the sensing ranges with few targets in sequence.

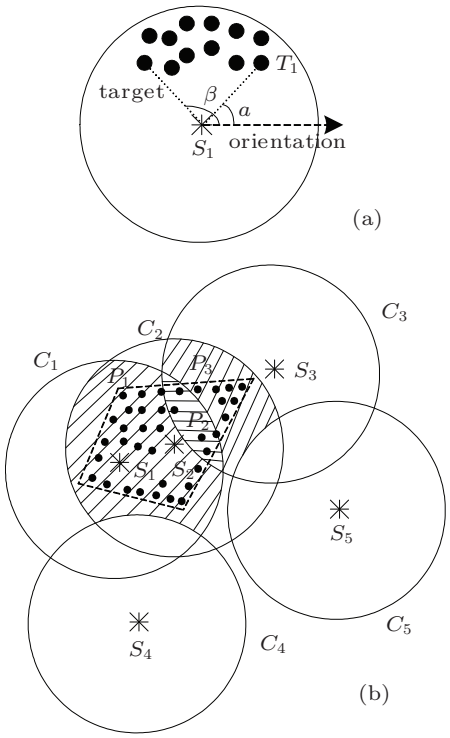


Fig. 1. Illustration for the ATTC: (a) the concept of AOA measurement and (b) a simple 5-sensor network.

As shown in Fig. 1(b), the angle range of a target within the sensing range of sensors S_1 is the largest, which is $[0, 360°]$. Hence we select S_1 to give a prior consideration in the next step.

Step 3 Find the patches which cover targets and are within the sensing range of the sensor obtained in Step 2

Some definitions used are given as follows:

1) S_n: a sensor whose identification (ID) is n;

2) C_n: the sensing range of S_n (a circle with S_n at the centre);

3) SR_{nm}: the angle range of the intersection of C_n and C_m relative to S_n;

We assume that C_n and C_m intersect at points A and B, and S_n is located at point C. The value

of SR_{nm} can be expressed as $[x, y]$. Then, x and y are denoted as directions of lines AC and BC with respect to the orientation, respectively;

4) AR_n: relative to S_n, the angle range of target within its sensing range;

5) TR_{nm}: relative to S_n, the angle range of target within the intersection of C_n and C_m.

Sensors satisfying the following two conditions should be found first.

i) Its sensing range intersects the sensing range of the sensor obtained in Step 2;

ii) There are several targets within the overlap between their sensing ranges.

The sensor obtained in Step 2 is denoted as S_i. Meanwhile, sensors meeting the two conditions are denoted as S_j, where i and j are the indexes of the related sensors. We assume that AR_j is $[\theta, \gamma]$ and SR_{ji} is $[\phi, \eta]$. The TR_{ji} is given by

$$TR_{ji} = \begin{cases} [\theta, \gamma], & \theta \geq \varphi, \gamma \leq \eta, \\ [\theta, \eta], & \varphi \leq \theta < \eta, \gamma \geq \eta, \\ [\varphi, \gamma], & \theta \leq \varphi, \varphi < \gamma \leq \eta, \\ [\varphi, \eta], & \theta \leq \varphi, \gamma \geq \eta, \\ 0, & \text{else.} \end{cases} \quad (1)$$

If the value of TR_{ji} is not equal to 0; it implies that there are targets within $C_i \cap C_j$. Then, based on the value of TR_{ji}, the values of S_j are arranged in a descending order, and stored in a table, namely the subordinate table of S_i. Patches covering targets and within $C_i \cap C_j$ are computed in sequence. That is, $C_i \cap C_j$ with a large value of TR_{ji} has a high probability of containing more patches. Hence, sensors S_j with large values of TR_{ji} are given prior consideration. Additionally, if several sensors have the same value of TR_{ji}, they are arranged in a random order.

In order to improve the accuracy of the estimated region, patches which are within $C_i \cap C_j$ and do not cover any target should be removed. These patches are named P_r. In order to find P_r, sensors whose sensing ranges intersect sensing regions C_i and C_j should be found. The set of these sensors is called I. Sensors belonging to I are called S_k. If the angle range of targets detected by S_k does not involve the angle range of $C_i \cap C_j \cap C_k$, it can be judged such that the region $C_i \cap C_j \cap C_k$ does not contain any target. Then the set of patches covering targets and within $C_i \cap C_j$ can be expressed as $C_i \cap C_j - P_r$.

As illustrated in Fig. 1(b), we first find patches covering targets within C_1. Sensors S_2 and S_3 meet the two conditions. Since $TR_{21} > TR_{31}$, patches within $C_1 \cap C_2$ and $C_1 \cap C_3$ are processed in sequence. As S_4 has not detected any target, $C_1 \cap C_2 \cap C_4$ does not cover any target. Meanwhile, it can be judged such that $C_1 \cap C_3$ is involved in $C_1 \cap C_2$ by simple geometric calculations. Hence, patches within $C_2 \cap C_1 - C_2 \cap C_1 \cap C_4$ must cover targets, which are P_1 and P_2.

Step 4 Find the patches within sensing ranges of other sensors and covering targets

Except sensors obtained by Step 2, based on the value of AR_n, sensors which have detected targets are arranged in a descending order, and stored in a table. Additionally, if several sensors have the same value of AR_n, they are arranged in a random order. In order to distinguish between this table and the table built in Step 3, we call them the major table and the subordinate table, respectively. Applying the computational procedures proposed in Step 3, patches covering targets and those within the sensing ranges of the sensors in the major table can be found in sequence. Two points should be paid attention to as follows.

a) Step 3 has explained how to find patches within the sensing range of the sensor obtained by Step 2. When the computational procedures in Step 3 are used in this step, the sensor obtained in Step 2 should be replaced by sensors in the major table.

b) Sensors should check patches obtained in the preceding steps. Patches which have been obtained are not considered in this step.

As demonstrated in Fig. 1(b), since $AR_2 > AR_3$, patches within C_2 and C_3 are processed in sequence. Since patches within $C_2 \cap C_1$ have been found in the previous step, this step needs to consider patches within $C_2 \cap C_3 - C_2 \cap C_3 \cap C_1$. Because S_5 has not detected any target, the patch within $C_2 \cap C_3 - C_2 \cap C_3 \cap C_1 - C_2 \cap C_3 \cap C_5$, namely P_3, must cover targets. To sum up, patches P_1, P_2, and P_3 construct the estimated region of the target group.

2.3. Discussion

The problem of tracking a target group can be modeled as tracking a geographical continuous region covered by all targets, but most single target tracking approaches are not suitable for this problem. As shown in Fig. 2, there is a single target in the monitoring region. Then, it can be judged such that the target must be in the patch $C_1 \cap C_2 \cap C_3$. However, as shown in Fig. 1(b), when there are several targets, it is hard to ascertain which patches cover these targets. Therefore, we introduce the AOA technique in

this paper. As mentioned in the assumption of the algorithm, to ensure ideal coverage, each sensor has 46 close neighbours. Patches are formed by overlaps between sensor sensing ranges. Hence, each sensor sensing range is divided into several patches. According to the angle range obtained by the AOA information and the geometry of patches, a sensor can find the patches covering targets. The set of these patches construct the estimated region of a target group. Therefore, the estimated region must have covered all the targets of the target group, and there are no targets outside the estimated region.

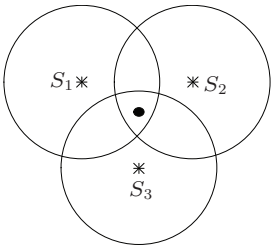


Fig. 2. Illustration for tracking a single target.

During the wireless communication, a message may be lost, but this problem is beyond the scope of this paper. However, a more serious problem may occur when some sensors in the WSN die. Under this circumstance, i.e., due to the deaths of some sensors, can the estimated region of the target group be still obtained using the ATTC? As mentioned before, each sensor has 4–6 neighbours. When a small number of sensors die, each sensor still has some neighbours and its sensing range will be divided into some patches. Then, the patches covering targets can be found using by the ATTC. Hence, the deaths of a few sensors will not affect the operation of the ATTC. But the accuracy of the ATTC will be reduced if many sensors die.

Based on the algorithm proposed in this section, a WSN is able to track a target group. Since the WSN samples the target group movement periodically, the ATTC provides snapshot results. A WSN can update the estimated region of the target group and let users obtain the spatiotemporal properties of the target group.

2.4. Performance analysis

In this section we analyse the minimum localization error which can be achieved using the ATTC. The localization error is defined as the difference in radius between the estimated region and the actual region of a target group.

Theorem 1 If the distance between each target and the logical centre is less than d_c, the error of localizing a target group is E_r, and the sensing radius of each sensor is R, then the E_r satisfies the inequality $0 < E_r < 2R$.

Proof We assume that the monitored field is greatly larger than R, so that we ignore the boundary behaviour by focusing on the portion of the monitored field that is at least R away from the boundary. Since the distance between each target and the logical centre is less than d_c, the targets of the target group must be within a circle at each time stamp, whose radius is d_c. As shown in Fig. 3(a), let O be the centre of circle D_1. This circle is defined as the actual region of a target group, and the diameter of the actual region is $2d_c$.

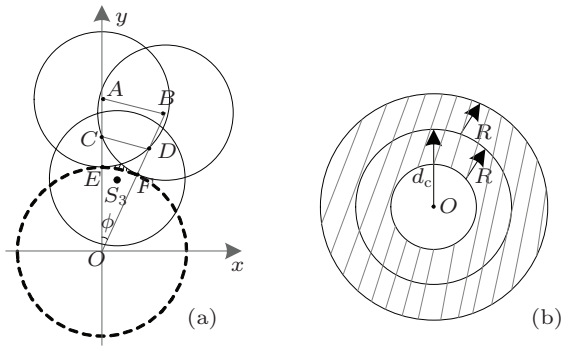


Fig. 3. Illustrations for Theorem1 and Theorem 2.

As mentioned in Subsection 2.2, the estimated region is the set of patches, which contains several targets. If parts of these patches have not covered any target, these parts are called blank regions (BRs). In order to obtain the minimum localization error, BRs should be covered by sensing ranges of sensors which have not detected any target. As shown in Fig. 3(a), the actual region is shown as the circle with dashed line. Points A and B represent locations of S_1 and S_2. The sensing ranges of S_1 and S_2 are tangential to this circle, so there are no targets in their ranges. Let S_3 represent a kind of sensor, part of whose sensing range is covered by targets. Hence, part of the sensing range of S_3 is outside D_1. Let the sensing ranges of S_1 and S_2 overlap with this region. Therefore, a patch covering targets, namely P_1, is formed, which is $C_3 - C_3 \cap C_1 - C_3 \cap C_2 + C_3 \cap C_1 \cap C_2$. The shaded section is one of the BRs within P_1, and the areas of several BRs dominate the localization error. The approaches to computing the area of the shaded section are as follows.

The coordinates of A and B are $(0, d_c + R)$, $((d_c + R)\sin\phi, (d_c + R)\cos\phi)$, respectively. Point C is the intersection point of C_2 and Y axis. Its coordinates are $(0, (d_c + R)\cos\phi - \sqrt{R^2 - (d_c + R)^2 \sin^2\phi})$, which are obtained by simple geometric calculations. Line CD is parallel to line AB. We can obtain

$$\left(\frac{OC}{OA}\right)^2 = \frac{S\Delta OCD}{S\Delta OAB}, \tag{2}$$

where $S_{\Delta OCD}$ and $S_{\Delta OAB}$ are the areas of triangles. Then we can obtain

$$S_{\Delta OCD} = \frac{1}{2}((d_c + R)\cos\phi - \sqrt{R^2 - (d_c + R)^2 \sin^2\phi})^2 \sin\phi. \tag{3}$$

To reduce the localization error, the area of the BR should be as small as possible. Hence, when the localization error is minimum, the value of ϕ satisfies the inequality

$$\phi < \delta, \tag{4}$$

where δ can be taken to be any positive value.

We use S_{BR} and S_{OEF} to note the areas of the shaded section and the sector OEF, respectively. Then we have

$$S_{BR} < S_{\Delta OCD} - S_{OEF} = S_{\Delta OCD} - \frac{\phi}{360^\circ}\pi d_c^2, \tag{5}$$

$$S_{\Delta OCD} < \frac{1}{2}((d_c + R) - \sqrt{R^2 - (d_c + R)^2\delta^2})^2\delta, \tag{6}$$

$$\frac{\phi}{360^\circ}\pi d_c^2 < \frac{\delta}{360^\circ}\pi d_c^2. \tag{7}$$

From Eqs. (5)–(7), we obtain Eqs. (8) and (9)

$$S_{BR} < \frac{1}{2} d_c^2 \delta, \tag{8}$$

$$\Rightarrow S_{BR} \approx 0. \tag{9}$$

If patches covering targets contain several BRs, and the deployment of several sensors makes the value of ϕ satisfy the following inequality:

$$\phi < \delta, \tag{10}$$

we can obtain

$$nS_{BR} \approx 0. \tag{11}$$

Since such BRs result in the localization error, the lower bound on the localization error is 0.

Let D_2 be the circle of radius $(d_c + R)$ centred at O. Only the sensors deployed in D_2 can sense targets within the target group. We use S_{estimate} and r_{estimate} to note the area and the radius of the estimated region, respectively. Then, we obtain the following inequalities:

$$S_{\text{estimate}} < \pi(d_c + 2R)^2, \tag{12}$$

$$\Rightarrow r_{\text{estimate}} < d_c + 2R, \tag{13}$$

$$\Rightarrow E_r < 2R. \tag{14}$$

To sum up, the E_r satisfies inequality

$$0 < E_r < 2R. \tag{15}$$

Theorem 2 If sensors are distributed according to the Poisson distribution of density ρ, the sensing radius of each sensor is R, and the distance between each target and the logical centre is less than d_c, then the localization error E_r satisfies the inequality

$$E_r < \Omega\left(\sqrt{\frac{(8\rho^2\pi^2R^4 - 2\rho\pi R^2 + 1)d_c R}{3}}\right)$$

under the condition of $R < d_c$, and

$$E_r < \Omega\left(\frac{\sqrt{3}}{6}(d_c + R)\sqrt{8\rho^2\pi^2R^4 - 2\rho\pi R^2 + 1}\right)$$

under the condition of $R > d_c$.

Proof As mentioned in Theorem 1, the actual region of a target group is defined as a circle D_1, and the radius of D_1 is d_c. As shown in Fig. 3(b), let D_2 be the circle of radius $(d_c + R)$. Circles D_1 and D_2 are both centred at O. Only the sensors deployed in D_2 can sense targets within the target group. The localization errors under two conditions are discussed below.

(I) The localization error under the condition of $R < d_c$

Let D_3 be the circle of radius $(d_c - R)$ centred at O. We observe that patches within the sensing ranges of sensors in D_3 are covered entirely by targets. It means that there are no BRs within these patches, and these patches will not result in localization error. As shown in Fig. 3(b), the sensing ranges of sensors within the shaded section contain many patches. We observe that these patches can be classified into three kinds: I) patches covered entirely by targets; II) patches which do not contain any target; III) patches which contain BRs. Hence, the area of BRs results in the localization error.

There are N sensors in the shaded section, where N can be obtained from the following expression:

$$N = \rho(\pi(d_c + R)^2 - \pi(d_c - R)^2) = 4\rho\pi d_c R. \tag{16}$$

We assume that a sensor S_1 is located at point A. Then sensors whose sensing range can overlap the sensing range of S_1, must be deployed in a circle of radius $2R$ centred at A. There are N_1 sensors in this

circle, where N_1 can be obtained from the following expression:

$$N_1 = \rho\pi(2R)^2. \tag{17}$$

The sensing ranges of the N_1 sensors can partition the sensing range of S_1 into at least (N_1+1) patches. The average area of a patch is given by

$$S_{\text{patch}} < \frac{\pi R^2}{N_1+1}. \tag{18}$$

On the other hand, it has been proposed in Ref. [7] that the sensing range of S_1 can be partitioned into at most $N_1^2 - N_1 + 2$ patches. Since two or more sensors may contain the same patch, the number of patches in sensing ranges of sensors in the shaded section satisfies

$$N_{\text{total}} < \frac{(N_1^2 - N_1 + 2)N}{2}. \tag{19}$$

The number of patches containing BRs is given by

$$N_{\text{patch}} < \frac{1}{3}N_{\text{total}}. \tag{20}$$

The area of these patches is given as follows:

$$S = N_{\text{patch}}S_{\text{patch}} < \frac{1}{3}\frac{(N_1^2 - N_1 + 2)N}{2}\frac{\pi R^2}{N_1+1}, \tag{21}$$

$$\Rightarrow S < \frac{2}{3}((4\rho\pi R^2)^2 - 4\rho\pi R^2 + 2) \rho\pi d_{\text{c}} R\frac{\pi R^2}{(4\rho\pi R^2+1)}, \tag{22}$$

$$\Rightarrow S < \frac{2}{3}((4\rho\pi R^2)^2 - 4\rho\pi R^2 + 2)\rho\pi d_{\text{c}} R\frac{\pi R^2}{4\rho\pi R^2}, \tag{23}$$

$$\Rightarrow S < \pi\frac{(8\rho^2\pi^2R^4 - 2\rho\pi R^2 + 1)d_{\text{c}}R}{3} = \Omega\left(\sqrt{\frac{(8\rho^2\pi^2R^4 - 2\rho\pi R^2 + 1)d_{\text{c}}R}{3}}\right). \tag{24}$$

Hence the radius of this area is at least

$$\Omega\left(\sqrt{\frac{(8\rho^2\pi^2R^4 - 2\rho\pi R^2 + 1)d_{\text{c}}R}{3}}\right).$$

Since the area of BRs in these patches results in the localization error, and the area S is larger than the area of BRs, the E_{r} satisfies the following inequality:

$$E_{\text{r}} < \Omega\left(\sqrt{\frac{(8\rho^2\pi^2R^4 - 2\rho\pi R^2 + 1)d_{\text{c}}R}{3}}\right). \tag{25}$$

(II) Localization error under the condition of $R > d_{\text{c}}$

Under the condition of $R > d_{\text{c}}$, patches within sensing ranges of sensors in D_2 can be classified into three kinds, which is the same as the classification under the condition of $R < d_{\text{c}}$. Applying the analytical method mentioned above, there are N_2 sensors in D_2, where N_2 can be obtained from the following expression:

$$N_2 = \rho\pi(d_{\text{c}} + R)^2. \tag{26}$$

Within the sensing ranges of these sensors, the number of patches containing BRs is given by

$$N_{\text{patch}} < \frac{1}{3}\frac{(N_1^2 - N_1 + 2)N_2}{2}. \tag{27}$$

The area of these patches is given by

$$S = N_{\text{patch}}S_{\text{patch}} < \frac{1}{3}\frac{(N_1^2 - N_1 + 2)N_2}{2}\frac{\pi R^2}{N_1+1}, \tag{28}$$

$$\Rightarrow S < \frac{1}{3}\frac{((4\rho\pi R^2)^2 - 4\rho\pi R^2 + 2)\rho\pi(d_{\text{c}} + R)^2}{2} \frac{\pi R^2}{4\rho\pi R^2}, \tag{29}$$

$$\Rightarrow S < \frac{1}{12}\pi(8\rho^2\pi^2R^4 - 2\rho\pi R^2 + 1)(d_{\text{c}} + R)^2. \tag{30}$$

Hence, the radius of this area is at least

$$\Omega\left(\frac{\sqrt{3}}{6}(d_{\text{c}} + R)\sqrt{8\rho^2\pi^2R^4 - 2\rho\pi R^2 + 1}\right),$$

and the E_{r} satisfies the following inequality (31):

$$E_{\text{r}} < \Omega\left(\frac{\sqrt{3}}{6}(d_{\text{c}}+R)\sqrt{8\rho^2\pi^2R^4 - 2\rho\pi R^2 + 1}\right). \tag{31}$$

3. Simulation results

In this section, we carry out extensive simulation tests to evaluate the performance of our algorithm. The code is written in Matlab. In our simulations, sensor nodes are distributed in a 1000×1000 grid according to Poisson distribution with density ρ. A target group follows the group mobility model within the field. We assume that a logical centre moves following a random waypoint model at a constant speed, and there are 50 individual targets moving around the logical centre. The only constraint is that the largest distance between a target and the logical centre is 45 units, which implies the radius of the actual region of a target group d_{c} is 45 units. We compare our proposed ATTC with the hull algorithm proposed in Ref. [13]. In the hull algorithm it is assumed that the region covering all plus sensors is the estimated monitoring region. We assume that the area of the estimated region is S. Then, the radius of the estimated region is defined as $\sqrt{S/\pi}$ in the simulation. The localization error is the difference in radius between the estimated region and the actual region of a target group.

For each simulation, we run the ATTC and the hull algorithm 10 times and use 10 random trajectories for the logical centre. The simulation results are then averaged to compute an average radius of the estimated region.

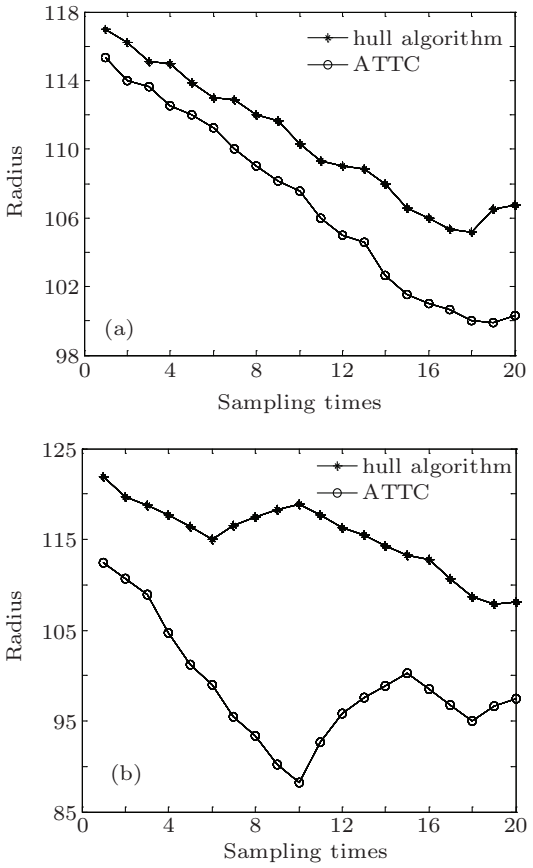


Fig. 4. Curves of estimated radius versus sampling time when $R = 40$ (a) and 50 (b).

The first two simulations concern the radii of the estimated region obtained by the ATTC and the hull algorithm at different sampling times. In this experiment, density ρ is kept constant at 9.5×10^{-4}, and the values of sensing radius R are kept constant at 40 units and 50 units in Figs. 4(a) and 4(b), respectively. Hence we can observe the radii of estimated region under the conditions of $R < d_c$ and $R > d_c$, respectively. The horizontal axis represents the moment during the movement of a target group. The vertical axis represents radius of the estimated region. The two figures show that the radius estimated by the ATTC is smaller than that estimated by the hull algorithm, which implies that the ATTC is more accurate in localizing a target group. The reason is that when a sensor has enough neighbour sensors within its sensing range, the area of each patch is very small. So the area of the region covering all plus sensors is larger than that of the set of patches containing several targets. The simulation results also support the bound of localization error deduced from Theorems 1 and 2.

The next two simulation experiments are for exploring the accuracy of the proposed algorithm for varying values of the sensor density ρ. We show the radii of the estimated region when the sensing radius is kept constant at 40 units and 50 units in Figs. 5(a) and 5(b), respectively. We can see that the localization accuracy of the ATTC has been improved as density increases. That is, when the number of sensors located within a unit area is small, the area of each patch is large. Hence the area of the set of patches covering targets may be larger than that of the region covering all plus sensors. Then the radius of the estimated region obtained by the ATTC may be larger than that obtained by the hull algorithm when the value of density is small. This result explains why the assumption in Section 2 points out that each sensor should have 4–6 close neighbours.

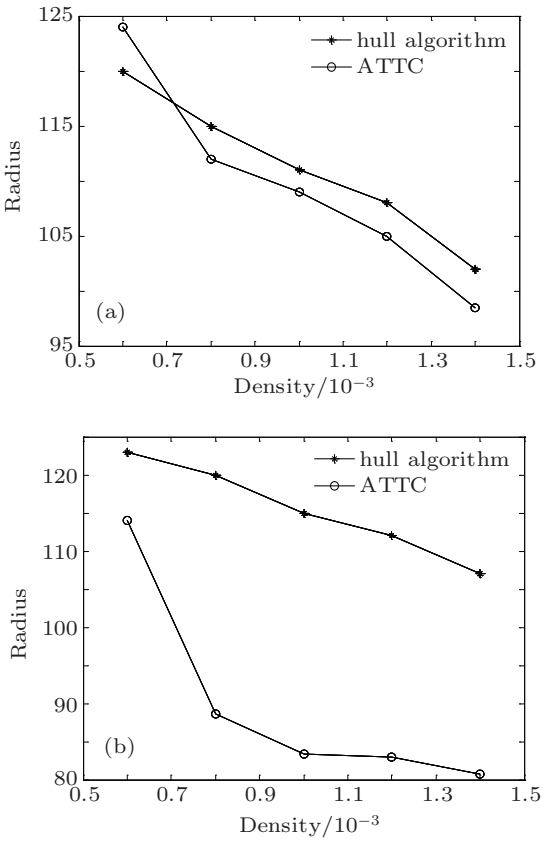


Fig. 5. Curves of estimated radius versus sensor density for $R = 40$ (a) and 50 (b).

The following simulations focus on the localization errors for varying values of sampling time and sensor density. Figures 6(a) and 6(b) show the curves of localization error versus values of sampling time and

ρ, respectively. The two figures show that the value of localization error is larger under the condition of $R < d_c$ than that under the condition of $R > d_c$. According to our analysis in Theorem 2, one of the patches must have an area of at least $\pi R^2/N_1^2$, where $N_1 = \rho\pi(2R)^2$. As R increases, the area of a patch decreases. Figure 7 highlights the influence of sensor density on the localization error. In the scenario of $R = 40$, the localization error ratio ATTC/hull algorithm falls from 105% to 93% as sensor density increases. This result indicates the overall descending tendency in the ratio with sensor density increasing. In addition, in the scenario of $R = 50$, the radio is always below 90%. Hence the increase of sensing radius results in the decrease of localization error.

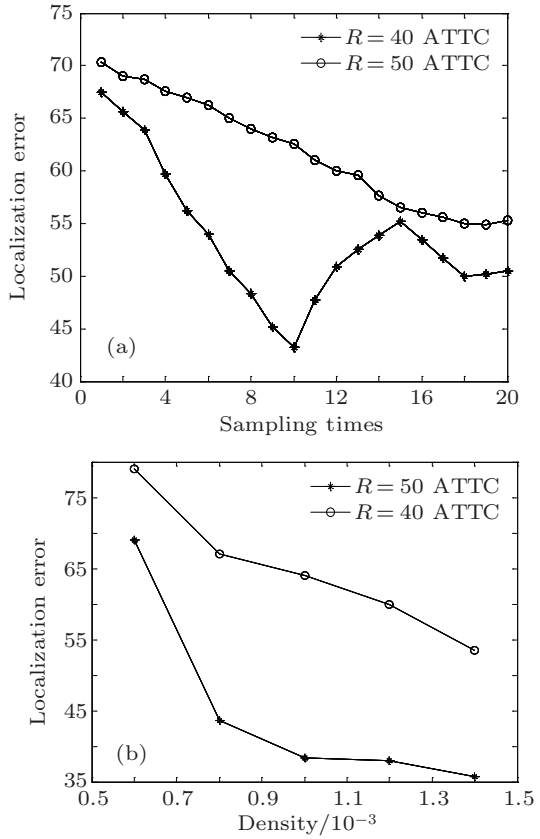


Fig. 6. Simulation curves of localization error versus sampling time (a) and sensor density (b).

Figure 8 shows a comparison between the energy consumptions of the ATTC and hull algorithms. In the two algorithms, the sensor observations are communicated to, and fused at, the sink node. The centralized architecture is implemented through multihop wireless communication between the sensors and the sink node. In order to analyse the difference caused by different tracking algorithms, the two algorithms should use the same routing approach. In our simulation, the DHAC proposed in Ref. [20] is used as the routing approach. The x axis and y axis of Fig. 8 represent the sensor density and the energy consumption of the WSN respectively. Simulation results show that the ATTC is more efficient than the hull algorithm. That is, the hull algorithm should scan sensors which have detected targets in the ascending order and discuss which sensors are the vertices of the desired convex hull. With the increase of sensor density, the number of sensors which have detected targets increases, and the WSN will consume much energy to compute and store a convex hull. Hence, with the increase of the sensor density, the ATTC offers a clear advantage.

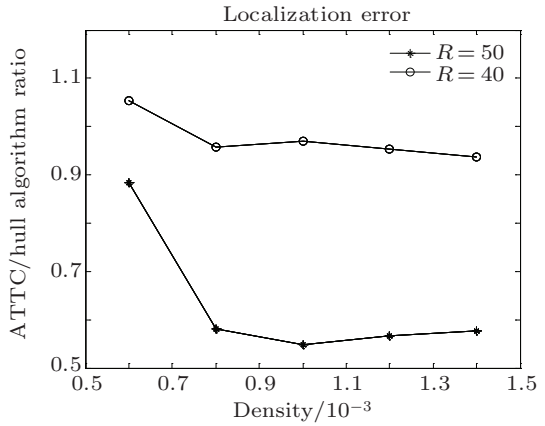


Fig. 7. Curves of ratio of ATTC to hull algorithm versus sensor density.

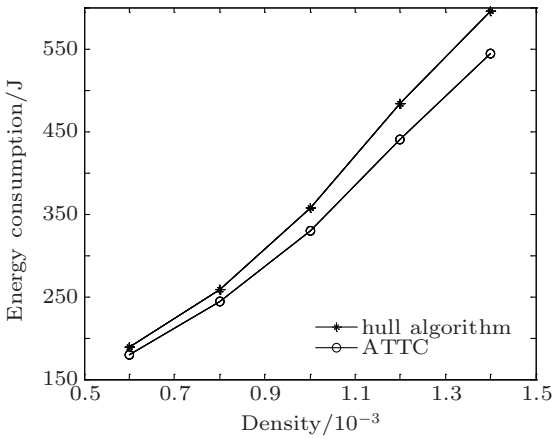


Fig. 8. Energy consumption versus sensor density.

4. Conclusions

This paper focuses on detecting, localizing, and tracking a target group with correlated motions. Since all targets are restricted within a limited region, the problem of tracking a target group can be modeled as tracking a geographical continuous region covered by

all targets. Based on the AOA information and locations of sensors, our tracking algorithm maintains the estimated region at each sampling time by exchanging messages among sensors. Furthermore, we explore fundamental performance limits to the accuracy of localizing a target group. Our simulation results show that the proposed tracking algorithm is superior to the existing hull algorithm in the sense of the reduction in location error.

References

[1] Tong X J, Wang Z and Zuo K 2012 *Chin. Phys.* B **21** 020506

[2] Chen M, Qiu M, Liao L X, Park J G and Ma J H 2011 *J. Supercomput.* **56** 353

[3] Wang N, Zhang Y D and Yuan P 2011 *Chin. Phys.* B **20** 074207

[4] Liang S, Zhang C X, Liu B, Lin W T, Li Q, Zhong X and Li L J 2010 *Chin. Phys.* B **19** 124217

[5] Yu A L 2008 *Chin. Phys.* B **17** 878

[6] Wei J and Zhang X 2009 28*th IEEE Conference on Military Communications*, October 2009, Boston, MA, p. 1

[7] Stanley M, Stephane G D and Adams J T *IEEE Sensors Applications Symposium*, February 7–9, 2012, Brescia, p. 56

[8] Sisinni, E, Archetti P, Manenti M and Piana E 2012 *IEEE Sensors Applications Symposium* February 7–9, 2012, Brescia, p. 98

[9] Lefevre S and Vincent N 2004 *Lecture Notes in Computer Science* p. 606

[10] Xu C and Prince J L 1998 *IEEE Trans. Image Process.* **7** 359

[11] Jin G A and Nittel S 2011 *Distrib. Parallel Databases* **29** 3

[12] Shrivastava N, Mudumbai R, Madhow U and Suri S 2006 4*th ACM Conference on Embedded Networked Sensor Systems*, October 31–November 3, 2006 Boulder, Colorado, USA, p. 251

[13] Cao D L, Jin B H, Das S K and Cao J N 2010 *J. Parallel Distrib. Comput.* **70** 825

[14] Anzai D, Yanagihara K, Lee K and Hara S 2011 *IEICE Trans. Commun.* **E94** B 1924

[15] Wen C Y and Chan F K 2010 *Sensors* **10** 9742

[16] Camp T, Boleng J and Davies V 2002 *Mobile & Wireless Communications* **2** 1

[17] Niculescu D and Nath B 2001 *IEEE Global Telecommunications Conference* November 25–29, 2001, San Antonio, TX, p. 2926

[18] Chizari H, Hosseini M, Poston T, Razak S A and Abdullan A H 2011 *Sensors* **11** 3163

[19] Verma S, Suryansh S and Kotwal S B 2010 *International Conference on Computational Intelligence and Communication Networks*, November 26–28, 2010, Bhopal, p. 301

[20] Lung C H and Zhou C 2010 *Ad Hoc Netw.* **8** 328